Pion and neutron production by cosmic-ray muons underground

Jean Delorme and Magda Ericson*
Institut de Physique Nucléaire et IN2P3, CNRS, Université Claude Bernard Lyon I, 43 Bd. du 11 Novembre, F-69622 Villeurbanne Cedex, France

Torleif Ericson†
Theory Division, CERN, CH-1211 Geneva 23, Switzerland

Petr Vogel
Physics Department, California Institute of Technology, Pasadena, California 91125
(Received 10 April 1995)

The production of positive pions and neutrons by cosmic muons at underground sites of various depths is investigated. We first test the equivalent photon method in the particular case of Δ excitation by the muon. We find that this method, when it neglects the momentum dependence of the transverse response, reproduces remarkably well the theoretical muon cross section. This success has lead us to apply the method to higher energies, where it has not been tested. We evaluate in this way the production of positive pions in liquid scintillator from known photo-absorption cross sections. At a shallow depth of 20 meters our estimate reproduces the measurement. As for the neutron emission, we include the obvious sources, such as the giant-resonance excitation, the quasideuteron process, the quasifree pion production as well as neutrons emitted following pion capture. Our evaluation underestimates the number of neutrons produced and finds a too weak dependence on the depth. This suggests that secondary neutron production is important at all depths.

PACS number(s): 96.40.Tv, 25.20.−x, 25.30.Mr, 25.40.Sc

I. INTRODUCTION

The passage of a high-energy charged particle through matter is an interesting source of electromagnetic nuclear reactions largely occurring at very small angles. One can view such processes as produced by the flux of a beam of nearly real equivalent photons [1–3]. Though these photons are virtual, their kinematics at small angles of deviation of the charged particle is so close to that of real photons that it becomes a good approximation to link the inelastic cross sections for charged particles to the ones for physical photons with an energy equal to the energy loss. The nuclear reactions induced by the small angle scattering of charged particles are of particular importance to low count rate underground experiments, such as searches for neutrino oscillations. The reason is that cosmic ray muons traverse the experimental area and their energy loss produces background neutrons and pions.

It is by no means a trivial matter to obtain reliable estimates for actual yields of neutrons and pions. The problem is related to the question of obtaining a sufficiently reliable estimate for the equivalent photon flux as well as to the problem of finding appropriate input data. This is the aim of the present investigation which has been stimulated by the rate of low-energy neutrons observed in an exploration of background sources in a planned neutrino oscillation experiment. As a quick estimate has shown, the neutron yield from the low-energy photonuclear giant-resonance excitation, as considered, e.g., in Ref. [4], is much too small to explain the observations, which suggests rather that meson-producing processes are primarily responsible. Indeed, negative pions are an efficient source of neutrons since most of them will slow down and stop in the surrounding matter. They are then captured into orbits of pionic atoms and produce neutron pairs by the quasideuteron absorption process $\pi^- + {}'d' \rightarrow 2n$ on the central nucleus. The observation of correlated neutrons is therefore linked to the yield of negative pions. To confirm this mechanism for neutron production we advocated a study of the yield of charged pions. Negative pions are not directly observable, but positive pions are produced at nearly the same rate. Their presence would be an indication in favor of this mechanism. The yield of positive pions has since been directly established experimentally from the observation of the delayed muon decay from the π^+ stopping without strong interactions [5].

For photons above 300 MeV an efficient way to produce pions is via the Δ isobar, which appears as a prominent peak in the photoabsorption cross sections. In view of the importance of the isobar region it is interesting to explore the validity of various approximations to the flux of equivalent photons there. In this case the isobar excitation by muons can be calculated without resorting to the equivalent photon method, and compared to the equivalent photon method in various limits as is done in Sec. II B, which follow the framework given in Sec. II A. This provides a guide for the application of this method at higher energies. In Sec. III we evaluate the π^+ production yield by high-energy muons utilizing the equivalent photon method. For this we need the photon partial cross sections for a given multiplicity of π^+ which, in turn, leads to the discussion of the assumptions

*Also at Theory Division, CERN, CH-1211 Geneva 23, Switzerland.

†Also at Institute of Theoretical Physics, P.O. Box 805, S-75105 Uppsala, Sweden.

necessary to deduce the yield of positive pions from experimental data. The somewhat unexpected result of this study is that pions are produced primarily above the Δ isobar region, often by multiple pion production.

II. EQUIVALENT PHOTON METHOD

A. General framework

We consider a charged lepton of mass m and initial momentum and energy $\mathbf{P}$, E scattering on a stationary target of mass M. The final lepton momentum and energy is $\mathbf{P}'$, E'. The energy and momentum transferred to the nucleus are, respectively,

$$\nu = E - E', \quad \mathbf{q} = \mathbf{P} - \mathbf{P}', \tag{1}$$

and θ is the laboratory scattering angle between $\mathbf{P}$ and $\mathbf{P}'$.

The double differential cross section in the laboratory frame is expressed in terms of the usual structure functions $W_{1,2}$. Here we adopt the convention used by Close [6], where they have the dimension [energy]$^{-1}$

$$\frac{d^2\sigma}{d\Omega dE'} = \frac{2\alpha^2}{Q^4}\frac{P'}{P}\left[(Q^2-2m^2)W_1 + \left(2EE' - \frac{Q^2}{2}\right)W_2\right], \tag{2}$$

where $Q^2 = \mathbf{q}^2 - \nu^2$. Now we introduce the transverse and longitudinal responses R_T and R_L defined by

$$W_1 = \frac{R_T}{2}, \quad W_2 = \frac{Q^4}{\mathbf{q}^4}R_L + \frac{Q^2}{2\mathbf{q}^2}R_T, \tag{3}$$

so that

$$\frac{d^2\sigma}{d\Omega dE'} = \alpha^2\frac{P'}{P}\left[\frac{4EE'-Q^2}{\mathbf{q}^4}R_L + \frac{4EE' + \mathbf{q}^2 + \nu^2 - 4m^2\mathbf{q}^2/Q^2}{2\mathbf{q}^2Q^2}R_T\right]. \tag{4}$$

To order $m^2/E^2 \ll 1$ we have

$$Q^2 \equiv \mathbf{q}^2 - \nu^2 \equiv (P-P')^2 - \nu^2 + 4PP'\sin^2\frac{\theta}{2} \simeq a^2 + 4EE'\left(1 - \frac{m^2}{EE'} - \frac{a^2}{2EE'}\right)\sin^2\frac{\theta}{2}, \tag{5}$$

where

$$a^2 = \frac{m^2\nu^2}{PP'} \simeq \frac{m^2\nu^2}{EE'} \ll \nu^2. \tag{6}$$

The allowed Q^2 values at different incident and transferred energies are shown in Fig. 1.

To make the link with the photoabsorption cross section, we define the effective number of photons $N(\nu)$ by

$$\frac{d\sigma}{dE'} = \int d\Omega \frac{d^2\sigma}{d\Omega dE'} = \frac{N(\nu)\sigma_\gamma(\nu)}{\nu}, \tag{7}$$

where the photon cross section σ_γ is related to the transverse response by [7]

$$\sigma_\gamma(\nu) = \frac{2\pi^2\alpha}{\nu}R_T(\nu, Q^2=0). \tag{8}$$

The simplest level of approximation neglects the longitudinal part of the response function and also ignores all momentum dependence of the transverse response, i.e., $R_T(\nu,Q^2) \cong R_T(\nu,Q^2=0)$. In this case the angular integration in Eq. (7) can be performed using

$$dQ^2 \equiv \frac{PP'd\Omega}{\pi}. \tag{9}$$

It leads to the formula

$$N(\nu) = \frac{\alpha}{\pi}\left[\frac{E^2+E'2}{P^2}\ln\frac{EE'+PP'-m^2}{m\nu} - \frac{(E+E')^2}{2P^2}\ln\frac{(P+P')^2}{(E+E')\nu} - \frac{P'}{P}\right], \tag{10}$$

which is nothing else than Eq. (1.7) of Dalitz and Yennie [3] (with the corrected sign in front of m^2).

It is appropriate here to make the link with the commonly used Weizsäcker-Williams method [8]. Starting with Eq. (4) we make the same assumptions as for the derivation of Eq. (10). Moreover, we put $E'/E \approx 1$ (i.e., a small energy loss), expand for small angles, $Q^2 \approx a^2 + EE'\theta^2$, $\mathbf{q}^2 \approx \nu^2 + EE'\theta^2$, and neglect $\mathbf{q}^2 + \nu^2$ with respect to $4EE'$, obtaining

$$\frac{d\sigma}{dE'} \approx \frac{2\pi\alpha^2 R_T(\nu,Q^2=0)}{\nu^2}\left[\ln\frac{1+E^4\theta_{\max}^2/m^2\nu^2}{1+E^2\theta_{\max}^2/\nu^2} - \frac{\theta_{\max}^2}{\theta_{\max}^2+\nu^2m^2/E^4}\right], \tag{11}$$

where $\theta_{\max}$ is a cutoff scattering angle. We also assume that $\theta_{\max} \gg m\nu/E^2 = a/E$ and therefore the effective photon number is

$$N(\nu) \simeq \frac{\alpha}{\pi}\left[2\ln\frac{\theta_{\max}E^2}{m(\nu^2+\theta_{\max}^2E^2)^{1/2}} - 1\right]. \tag{12}$$

This is now the formula that can be compared to the Weizsäcker-Williams method [8]:

$$N(\nu) = \frac{\alpha}{\pi}\frac{c^2}{v^2}\left[2\ln\frac{1.123p}{m\nu b_{\min}} - \frac{v^2}{c^2}\right]. \tag{13}$$

Here $v \simeq c$ is the muon velocity, p its momentum, and $b_{\min}$ is the minimum impact parameter. Formula (13) is essentially equivalent to our Eq. (12) provided we identify $b_{\min} = 1/E\,\theta_{\max}$ for $\theta_{\max} < \nu/E$ and $b_{\min} = 1/\nu$ for $\theta_{\max} > \nu/E$.

Moreover, Eq. (12) is identical to Eq. (1.7) of Dalitz and Yennie [3] and our Eq. (10) if we take $\theta_{\max} = \nu/E$, and assume that $\nu \ll E$. In fact, the integral over $d\Omega$ leading to Eq. (10) gets the largest contributions from scattering angles $\theta \leq \nu/E$ and saturates at $\theta \simeq \nu/E$, which justifies the identification $\theta_{\max} = \nu/E$ above, and is compatible with our assumption that that $\theta_{\max} \gg a/E$. Equations (12) and (13) become therefore equivalent when we take $b_{\min} = 1/\nu$, while Ref. [8] suggests instead the identification of $b_{\min}$ with the larger of the quantities $1/E$ or R, where R is the nuclear radius. The presence of an undetermined parameter $b_{\min}$ is a serious drawback of the classical Weizäcker-Williams method, and its absence makes Eq. (10) attractive.

The real question is whether our assumption that

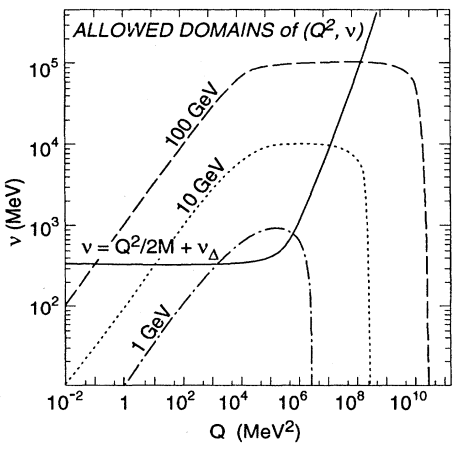

FIG. 1. Boundaries of the allowed domain of Q^2 vs ν for different muon energies (dot-dashed lines). The solid line represents the region of nonvanishing response for Δ excitation. The intersections betwen the solid and dot-dashed lines determine the $Q^2_{\min}$ and $Q^2_{\max}$.

$$R_T(\nu,Q^2 \leq \nu^2) \simeq R_T(\nu,Q^2=0) \tag{14}$$

is justified. To establish this, the following section explores this question for quasielastic Δ excitation for which the photon number can be calculated exactly, which allows tests of various approximations.

B. Test of the method for Δ resonance production

1. Nucleons at rest

The choice of the Δ resonance is guided by two considerations. First, it is a prominent feature in the photoabsorption cross section. Second, in a given model it is tractable exactly. It can therefore be used as a test for different approximations to the equivalent photon method. This study will be done under the assumption that the Δ isobar has no width. We also ignore the quadrupole excitation of the Δ resonance; i.e., we take the longitudinal response to vanish. In a first step we omit the Fermi motion of the nucleons. It is introduced later with no major change in the conclusions. With these assumptions the transverse nuclear response per nucleon R_T for Δ resonance excitation has the following form, according to Chanfray *et al.* [9]:

$$R_T \approx \tfrac{2}{9}G_{M*}^2(Q^2)\frac{(M^*-M)^2+Q^2}{4M^2}\,\delta\left(\nu-\nu_\Delta-\frac{Q^2}{2M}\right), \tag{15a}$$

$$= \tfrac{2}{9}G_{M*}^2(Q^2)\frac{\mathbf{q}^2}{(M^*+M)^2+Q^2}\,\delta\left(\nu-\nu_\Delta-\frac{Q^2}{2M}\right), \tag{15b}$$

where $\nu_\Delta = (M^{*2}-M^2)/2M$, while $M^*(M)$ is the Δ (nucleon) mass and $G_{M*}(Q^2)$ the $N\Delta$ transition form factor. We use $G_{M*}(0) = \mu^*[(M^*+M)/2M]^2$ with $\mu^* = 2\mu_V = 2\times 4.71$ nm, and assume the usual dipole form for its Q^2 dependence with the standard cutoff parameter $\Lambda = 6m_\pi$. The response depends obviously on Q^2, not only because it has magnetic character but also because of the recoil effect. In addition, there is of course the Q^2 dependence coming from the vertex form factor. Substituting for R_T in Eq. (4) (where we have taken $R_L = 0$) we can integrate over $d\Omega$, alternatively over dQ^2, using Eq. (9). Note that since we treat the Δ as a sharp state, we cannot use directly the relation (7) between the photon cross section, $\sigma_\gamma(\nu)$, and the differential cross section for muons, $d\sigma/dE'$, to define an effective photon number $N(\nu)$ depending on the energy loss. Indeed, due to recoil effects, the muon cross section is shifted to a somewhat different energy with respect to the photon one. The number of equivalent photons can be defined only from the energy-integrated cross sections, as follows:

$$N_\gamma = \frac{\int dE'\, d\sigma(E')/dE'}{\int d\nu\, \sigma_\gamma(\nu)/\nu}. \tag{16}$$

Therefore the total cross section for Δ resonance excitation is needed, and it is obtained by integrating again Eq. (4) over the final energy E' (i.e., over the excitation energy ν). The domain of integration in the (Q^2,ν) plane is determined by two requirements. First, the argument of the δ function defines the dispersion line

$$\nu=\frac{Q^2}{2M}+\nu_\Delta \tag{17}$$

outside of which the response vanishes (see the solid line in Fig. 1). Second, the kinematical conditions of muon scattering (5) restrict the variation of Q^2 between minimum and maximum values attained at 0° and 180°. It is then easily found that one has only access to the part of the (Q^2,ν) plane lying below the line defined by

$$\nu=\frac{1}{2m^2}[-EQ^2+P\sqrt{Q^2(Q^2+4m^2)}]. \tag{18}$$

This is illustrated for muons of different energy by the dashed curves in Fig. 1. They rise from 0 to the maximum energy loss $\nu_M=E-m$ which is attained for $Q_M^2=2m(E-m)$, and then decreases to 0 again at the maximum possible transfer $4P^2$. At lepton energies above the Δ excitation threshold they intersect the dispersion line of Eq. (17) twice. The intersection points define the limits of the domain of integration along this line and therefore determine $Q^2_{\min}$ and $Q^2_{\max}$ These are given by the roots of the equation

$$Q^4\left(\frac{2E}{M}+1+\frac{m^2}{M^2}\right)-4Q^2\left[P^2-\frac{\nu_\Delta}{M}(EM+m^2)\right]+4m^2\nu_\Delta^2=0, \tag{19}$$

which are approximately

$$Q^2_{\min}\approx\frac{m^2\nu_\Delta^2}{E(E-\nu_\Delta)}\,,\quad Q^2_{\max}\approx\frac{2E(E-\nu_\Delta)M}{(E+M/2)}\,. \tag{20}$$

The value of $Q^2_{\min}$ decreases rapidly with increasing energy E as seen in Fig. 1. We find for example the values 392, 13, and 0.13 $(\mathrm{MeV}/c)^2$ for $Q^2_{\min}$ for the incident energies $E=2$, 10, and 100 GeV, respectively. The region close to this limit dominates the integral, since the cross section is sharply peaked at small angles [see Eq. (4)]. For real photons the cross section for a Δ excitation of negligible width is

$$\sigma_\gamma(\nu)=\frac{2\pi^2\alpha}{\nu}R_T(Q^2=0,\nu)=\frac{4\pi^2\alpha}{9}G^2_{M*}(Q^2=0)\frac{(M^*-M)}{2M(M^*+M)}\delta(\nu-\nu_\Delta), \tag{21}$$

with its inverse energy-weighted integral

$$\int d\nu\sigma_\gamma(\nu)/\nu=\frac{4\pi^2\alpha}{9}\frac{G^2_{M*}(Q^2=0)}{(M^*+M)^2}\,. \tag{22}$$

The equivalent photon number deduced through Eq. (16) from our calculated muon and photon cross sections is an exact one within the model. It can be compared with various approximations given by Dalitz and Yennie, in particular Eq. (10) obtained under the assumption of a momentum-independent transverse response. This expression which is a function of the energy has to be evaluated at the excitation energy ν_Δ of the Δ isobar by photons. This comparison is summarized in Table I for muons of different energies. Surprisingly the agreement between our exact photon number and the one given by the Dalitz-Yennie formula (10) is excellent, well beyond what is expected from the Q^2 dependence of the response. In order to elucidate the origin of this intriguing agreement we have proceeded in several steps.

TABLE I. Number N_γ of equivalent photons for Δ excitation by muons ($\times 100$). The lines correspond to (a) R_T = const, corresponding to the Dalitz-Yennie "standard value," Ref. [3] Eq. (1.7), (b) R_T = const $\times\mathbf{q}^2$ corresponding to Dalitz-Yennie Eq. (1.8), (c) full expression for R_T with standard cutoff value $\Lambda=6m_\pi$, (d) full expression for R_T, $\Lambda=8m_\pi$, and (e) full expression for R_T, $\Lambda=\infty$ (pointlike vertex).

E (GeV)	2	5	10	20	50	100
(a)	0.93	1.44	1.81	2.16	2.61	2.94
(b)	2.05	3.11	3.86	4.56	5.46	6.12
(c)	0.90	1.42	1.79	2.15	2.59	2.92
(d)	1.00	1.53	1.91	2.27	2.72	3.05
(e)	1.38	2.07	2.52	2.93	3.42	3.77

TABLE II. Number N_γ of equivalent photons for Δ excitation by muons ($\times 100$). The lines correspond to (a) R_T = const $\times\ \mathbf{q}^2$, (b) R_T = const $\times\ \mathbf{q}^2\delta(\nu-\nu_\Delta-Q^2/2M)$, and (c) R_T = const $\times\mathbf{q}^2/[(M^*+M)^2+Q^2]$.

E (GeV)	2	5	10	20	50	100
(a)	2.05	3.11	3.86	4.56	5.46	6.12
(b)	1.45	2.23	2.79	3.31	3.98	4.48
(c)	1.68	2.27	2.65	3.01	3.47	3.87

TABLE III. The influence of form factor variation on the photon number for different parts of the response Eq. (15a). The upper numbers of each entry are calculated with a constant form factor ($\Lambda=\infty$); the second ones in parentheses include the form factor variation with a cutoff parameter $\Lambda=6m_\pi$. (a) R_T = const $\times G_M^*(Q^2)$ (the first line reproduces Dalitz-Yennie "standard value"), (b) R_T = const $\times G_M^*(Q^2)\times\delta(\nu-\nu_\Delta-Q^2/2M)$, and (c) R_T = const $\times G_M^*(Q^2)\times Q^2\times\delta(\nu-\nu_\Delta-Q^2/2M)$. Note that adding lines (b) and (c) gives back lines (c) and (e) of Table I as it should.

μ energy (GeV)	2	5	10	20	50	100
(a)	0.93	1.44	1.81	2.16	2.61	2.94
	(0.75)	(1.25)	(1.61)	(1.96)	(2.40)	(2.73)
(b)	0.84	1.36	1.72	2.08	2.52	2.86
	(0.71)	(1.21)	(1.57)	(1.92)	(2.36)	(2.69)
(c)	0.54	0.71	0.80	0.85	0.90	0.92
	(0.19)	(0.21)	(0.22)	(0.23)	(0.23)	(0.23)

First, we have suppressed one obvious source of Q^2 dependence of the response in our calculation, namely, that of the magnetic form factor that we now take to be constant. As shown in Table I, this has a sizable effect since this suppression increases the muon cross section by about 30–40 %, destroying the previous agreement.

It is then natural to try to cure this problem by using instead the formula (1.8) of Dalitz and Yennie [3], appropriate for a magnetic transition with a response proportional to $\mathbf{q}^2$ and no further momentum dependence:

$$N(\nu)=\alpha\pi\frac{E^2+E'2}{P^2}\ln\frac{EE'+PP'-m^2}{m\nu}. \tag{23}$$

It turns out that this approximation is a poor one. It does not reproduce our exact result even when we use a constant form factor (see Table II). The reason is that the response is not only proportional to $\mathbf{q}^2$, but there are additional sources of momentum dependence, as seen in the second form of the response, Eq. (15b). Their effect is sizable. This is illustrated in Table II: In line (b) we introduce the recoil effect in the energy conserving δ function, which produces a momentum dependence. In line (c), instead, we introduce the momentum dependence of the denominator of Eq. (15b), which acts as a form factor. Both have the effect of reducing the muon cross section by sizable amounts. Therefore, the expression (23), which in principle should be more appropriate for a magnetic transition, is in fact a poor approximation. Equation (10) (the Dalitz-Yennie "standard value"), which assumes a constant response, agrees much better with our result, in particular with the one where the variation of the form factor is kept. The reason is that the decrease of the form factor cuts off the large momenta and makes the assumption of a constant response better which leads to the agreement with formula

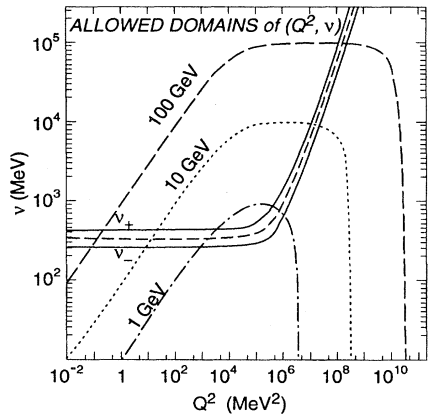

FIG. 2. Same caption as Fig. 1 with account of Fermi motion. The region of nonvanishing response now lies between the two solid curves (calculated with p_F = 230 MeV/c) which come to coincide with the dispersion line (17) in the limit p_F = 0 (dotted curve). There are four intersections between the solid and dot-dashed lines which determine the bounds of the integration region.

(10). We have checked this by exploring the influence of the form factor on the constant term $(M^*-M)^2$ of the response in Eq. (15a) and on the Q^2 part [see lines (b) and (c) of Table III]. Notice that the first numbers in line (a) reproduce those of line (a) of Table I with a constant response. While the form factor influence is only moderate on the first part, it is quite large in the Q^2 term, which is strongly suppressed. This makes the approximation of a constant response a valid one. A good agreement between our value and the formula (10) is therefore understandable, although such a perfect one is a coincidence depending on the exact value of the cutoff parameter. This is illustrated by line (d) in Table I where we have used a larger value $\Lambda=8m_\pi$. The agreement remains good although not quite perfect. It is difficult to prove the general validity of the Dalitz-Yennie formula for other production mechanisms. Consequently, one cannot give a universal expression for the equivalent photon number, which allows the derivation of the muon cross section from the photon one with good accuracy. In the absence of this universal relation and in view of the good agreement provided by the expression (1.7) of Ref. [3] we have thus used it at all energies and, in particular, also in the multipion range. The accuracy of such an approximation is obviously difficult to assess.

2. *Effect of Fermi motion*

We investigate now the influence of the Fermi motion of the nucleons. The nuclear response in the (Q^2,ν) plane is no longer restricted by Eq. (17) to the line $\nu=Q^2/2M+\nu_\Delta$ (dotted line in Fig. 2), but now falls in a band between the two curves (the solid lines in Fig. 2),

$$\nu_\pm=\frac{1}{2M^2}[E_F(Q^2+2M\nu_\Delta)\pm p_F\sqrt{4M^2Q^2+(Q^2+2M\nu_\Delta)^2}], \tag{24}$$

where p_F and E_F are the Fermi momentum and energy ($E_F=\sqrt{M^2+p_F^2}$). They meet the vertical axis at $\nu_\pm(0)=(E_F\pm p_F)\nu_\Delta/M$. Each of them has two intersections with the kinematical line (18) which limits the accessible part of the (Q^2,ν) plane. The integration domain is thus now a surface delineated by four sections of curves. In the variable Q^2 the abscissas of the intersection points are defined by the roots of equations

$$Q^4\left[\frac{2(EE_F\pm Pp_F)}{M^2}+1+\frac{m^2}{M^2}\right]-4Q^2\left[\frac{(PE_F\pm Ep_F)^2}{M^2}-\nu_\Delta\frac{(EE_F\mp Pp_F+m^2)}{M}\right]+4m^2\nu_\Delta^2=0, \tag{25}$$

which give back Eq. (19) in the limit $p_F=0$. The corresponding values of ν are obtained by substitution of the solutions in Eq. (18) or (24).

We have made the estimate with a Fermi momentum of 230 MeV/c, which is a characteristic value for a light nucleus like carbon, and using the analytic expressions for the response of a Fermi gas given in Ref. [9]. The resulting effect of Fermi motion on the average photon number N_γ is unimportant at lower lepton energies, and it represents only a 2.5% effect at 15 GeV. It becomes non-negligible in the region of 30 GeV and above. The vicinity of the singularity makes the integral sensitive to the detailed behavior of the integrand and thus to Fermi spreading so that N_γ deviates somewhat from its free nucleon value. We find, for instance, a decrease of the photon number by 6%, 11%, 19%, and 27% at 20, 30, 50, and 100 GeV, respectively.

III. APPLICATION

We now turn to the application of the equivalent photon method to the production of pions and neutrons by the cosmic ray muons underground. The muon flux at a depth d, $f_d(E)$, normalized according to $\int f_d(E)dE=1$, can be obtained from the spectrum on surface as given in Ref. [10], taking into account the energy losses of muons penetrating to a given depth. In Fig. 3 we show the normalized muon flux for various shallow depths. The corresponding total fluxes (in units of muons per horizontal area of one m^2 per second) are 131 for $d=0$, 33 for $d=20$ m, 12 for $d=50$ m, and 3.4 for $d=100$ m. One sees that the muon spectrum hardens with depth; the average muon energies are increasing and for the considered d values we get $\langle E\rangle$ = 5.4, 10.3, 13.5, and 22.4 GeV. At the depth of 500 m the flux is reduced to 0.082 muons/(m^2 s) and $\langle E\rangle$ = 80 GeV.

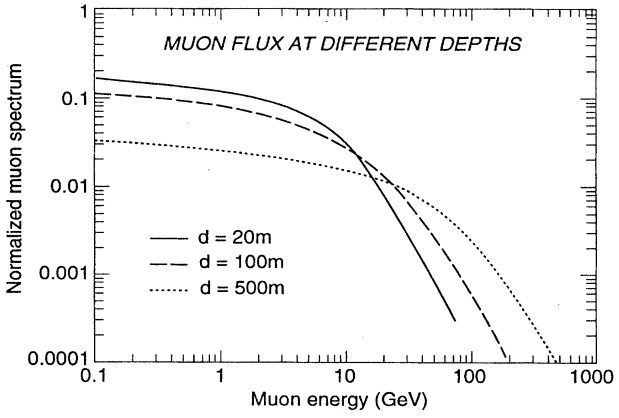

FIG. 3. Normalized muon flux at different depths.

By folding the muon flux $f_d(E)$ with $N(\nu)$, Eq. (10) or alternatively Eq. (12), we obtain the dimensionless effective number of equivalent photons (per muon) of a given energy at a given depth:

$$\mathcal{N}_d(\nu)=\int_{m+\nu}^{\infty}N(\nu)f_d(E)dE. \tag{26}$$

In Fig. 4 we show the effective photon number $\mathcal{N}_d(\nu)$ at different depths for photon energies up to 100 GeV. In preparing the figure we used Eq. (10); the results for Eq. (12) with $\theta_{\max}=\nu/E$ are, naturally, very similar. Notice that $\mathcal{N}_d(\nu)$ is at first approximatively constant as a function of ν. The horizontal part turns into a steep decrease for ν somewhat less than $\langle E\rangle$, where it is cut off by the decreasing muon spectrum. As a function of depth the horizontal part of $\mathcal{N}_d(\nu)$ increases as $\ln(\langle E\rangle)$, as expected. The photon energy where $\mathcal{N}_d(\nu)$ bends down increases, however, linearly with the average muon energy $\langle E\rangle$. In Fig. 4 we used Eq. (10) for $N(\nu)$ even very close the lower integration limit in Eq. (26), where its application is somewhat suspect, because the corresponding scattering angle is not small. That region contributes relatively little to the integral, however.

In Sec. II A 1 we have shown that Eq. (10) relates correctly the muon-nucleus cross section to the photonuclear cross section in the Δ resonance region. Here we are in a position to justify, at least approximately, its application also

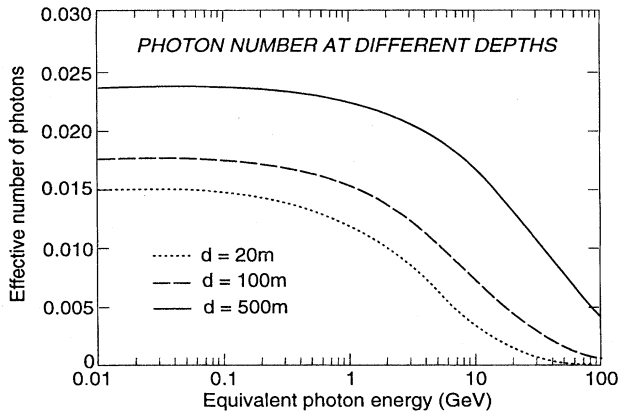

FIG. 4. Effective photon number at different depths according to the dimensionless definition in Eq. (26), per muon. [For the general definition of $N(\nu)$ see Eq. (7). $N(\nu)$ is the number of equivalent photons per unit energy times the photon energy.]

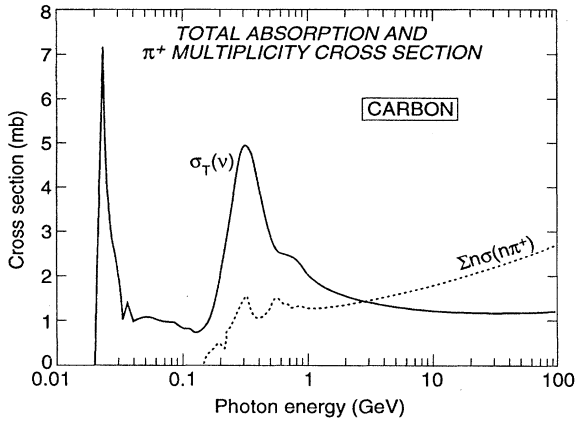

FIG. 5. Total photoabsorption cross section for carbon (solid line) and the weighted π^+ photoproduction cross section $\Sigma_n n\sigma(n\pi^+)$ (dashed line).

in the higher-energy region. According to the standard treatment [10,11] the muon energy loss by interaction with nuclei is governed by the formula

$$\frac{dE}{dX} = -b_{\text{nuc}}E, \tag{27}$$

where b_{nuc} is approximately independent of muon energy, and equal to $\approx 0.5\times 10^{-6}$ per g/cm^2. Using Eq. (10), the photoabsorption cross section in Fig. 5, and integrating over the photon energy, we can calculate b_{nuc}. The quantity b_{nuc} calculated this way is indeed almost independent of the muon energy for 1 GeV $\leq E \leq$ 100 GeV (it is very slowly rising, by a factor of less than 2), and its magnitude agrees with the empirical value within its uncertainties.

The reaction cross section in a given exit channel, averaged over the muon spectrum at a given depth d, is obtained by analogy to Eq. (7),

$$\frac{d\sigma}{d\nu} = \frac{\mathcal{N}_d(\nu)\sigma_\gamma(\nu)br(\nu)}{\nu}, \tag{28}$$

where $br(\nu)$ is the branching ratio for the corresponding reaction channel, e.g., (γ,n), (γ,π^+), etc. (If more than one particle of a given kind can be produced, the branching ratio should also reflect the corresponding multiplicity; see below.) The cross section (28) gives the number of neutrons, π^+, etc., produced per muon at the depth d in the *primary* reaction. As we pointed out in the Introduction, additional particles, in particular neutrons, can be produced in secondary reactions. Thus, the yields obtained with Eq. (28) are really lower limits for the neutron production. In order to apply the formalism we have to substitute in Eq. (28) the corresponding experimental photonuclear cross sections and branching ratios.

The total photoabsorption cross section which we used is shown in Fig. 5. Since the (γ,n) reaction is the only reaction channel of interest for photon energies below the pion production threshold, we use this partial cross section at these energies, and the full cross section above it. The data are from Ref. [12] for the giant-resonance region and from Ref. [13] above it. The data are smoothed at higher energies and extrapolated at very high energies.

We first consider the pion production, which can be evaluated more reliably. For this we require the branching ratio $br(\nu)$ for π^+ and π^- in the Δ resonance region ν = 160–500 MeV, and in the higher-energy region above. In the high-energy region the analysis is simplified by the empirical observation that the photoproduction cross section of π^+ and π^- on a proton is nearly the same as the corresponding one on a neutron with the opposite charges for the pions. For example, the cross section for the reaction $\gamma+p\rightarrow\pi^+ +\pi^- +p$ is approximately equal to the cross section for $\gamma+n\rightarrow\pi^- +\pi^+ +n$, and similarly for $\gamma+p\rightarrow\pi^+ +\pi^0 +n$ and $\gamma+n\rightarrow\pi^- +\pi^0 +p$. This feature follows from isospin invariance if one of the two isospin components is negligible. This near equality is observed for all pion producing reactions of interest. This means that we do not need all partial cross sections, and in particular, that for a carbon target the number of π^+ produced is the same one as the number of π^-.

Since for photon energies above 1 GeV multipion production becomes important, the proper definition of the branching ratio br(ν) for pions is

$$\text{br}(\nu) = \frac{\Sigma_n n\sigma(n\pi^+)}{\sigma_{\text{tot}}}. \tag{29}$$

The π^- production has the same branching ratio in carbon, as we just pointed out above.

For photon energies below 1 GeV the reactions $\gamma+p\rightarrow\pi^+ +n$, $\gamma+p\rightarrow\pi^+ +\pi^0 +n$, and $\gamma+p\rightarrow\pi^+ +\pi^- +p$ (and the corresponding ones for the neutron targets) are known and are the only ones of interest. For photon energies between 1 and 10 GeV we were able to find the data for the proton and deuterium targets only at a few isolated photon energies [14]. The corresponding branching ratio appears to be, however, a smooth and relatively slowly increasing function of energy. Thus we interpolated between the known points. Finally, to extend to even higher photon energies we extrapolated this smooth trend linearly in the logarithm of the photon energy. It is encouraging to note that such an extrapolation leads to an average π^+ multiplicity of about 2.5 at the photon energy of 100 GeV, in a good agreement with the measurement of Enikeev *et al.* [16] for the electromagnetic showers of similar energy (note, however, that our slope of multiplicity versus energy is less than the one measured in Ref. [16] at considerably higher energies 100–1000 GeV).

Having determined the branching ratio br(ν) for the nucleon targets, we assume that in nuclear targets (in our case in carbon) the same br(ν) is applicable. Thus the quantity $\Sigma_n n\sigma(n\pi^+)$ is obtained by multiplying $br(\nu)$ for nucleons by the total photoabsorption cross section for carbon. The dashed curve in Fig. 5 shows this $\Sigma_n n\sigma(n\pi^+)$. The rather uncertain cross sections and branching ratios at the highest energies are, fortunately, not very important for our final results at shallow depths. This uncertainty, however, prevents us from extending the calculations to deeper sites.

It is now a simple matter to evaluate the π^+ production yield by integrating Eq. (28) over the virtual photon energy ν. The results are presented in Table IV. We divide there the

TABLE IV. Summary of the π^+ production yields in the liquid scintillator [in units of $10^{-6}\pi^+$ per muon and per (g cm^{-2})]. The first entry in each column is for the carbon component, and the second entry in parentheses is for the hydrogen component.

Depth	Δ resonance 0–0.5 GeV		High energy 0.5–10 GeV		Asymptotic 10–100 GeV		Total	
	C	H	C	H	C	H	C	H
20 m	0.62	(0.16)	1.62	(0.34)	0.18	(0.04)	2.42	(0.54)
100 m	0.75	(0.20)	2.30	(0.48)	0.61	(0.12)	3.66	(0.80)
500 m	1.05	(0.27)	3.79	(0.78)	2.22	(0.45)	7.06	(1.50)

contributions to the integral into three energy bins. Column 2 demonstrates that the Δ resonance contributes relatively little, even at very shallow depths. For $d = 20$ and 100 m the bulk of the contribution comes from the region below 10 GeV (column 3), where the multiplicities and cross sections are reasonably well known. For the largest depth ($d = 500$ m) there is a large contribution from photons of 10–100 GeV and contributions from energies beyond 100 GeV, which are not included, will increase the total cross section even further.

Since we want to compare our calculated pion yield with the measured one in a liquid scintillator, we have to take into account the large hydrogen component of the scintillator (H/C ratio of 1.89). The calculation of the pion yield from the muon scattering on protons proceeds in a complete analogy with the calculation for carbon described above. The cross sections and branching ratios are taken from Ref. [14], and the resulting pion yields are quoted in Table IV (the entries in parentheses).

In Table IV we express the π^+ yield in the units in which it is usually measured, i.e., the number of particles per muon and per (g cm^{-2}). To transform the cross section into such units we have to multiply it by the number of carbon nuclei per gram of scintillator, $N_C = 4.3\times10^{22}$ g^{-1}, and analogously by the number of hydrogen nuclei per gram, $N_H = 8.2\times10^{22}$ g^{-1}. It is very encouraging to note that our total yield (i.e., adding the carbon and hydrogen contributions) is 2.95×10^{-6} at $d = 20$ m in agreement within errors with the yield $3.5\pm0.7\times10^{-6}$ measured at that depth in Ref. [5].

According to our calculation the pion yield should increase by a factor of 3 when going from $d = 20$ m to 500 m. The depth dependence has not been measured for pion production and would constitute a test of the validity of our approach.

The analogous calculation for the total yield of neutrons is much more problematic, in particular at deeper depths corresponding to high-energy photons. The reason is the importance of neutron production by secondary spallation processes. Another uncertainty arises from the possible direct neutron production through virtual pion creation and absorption [15], although we believe that such an effect is small in carbon. We do not treat the secondary processes here, but we comment below on a possible more complete treatment of the neutron production. First however, since the global neutron yield is of considerable practical importance to underground physics and some data exist [5,16,17], we give here a crude estimate recalling that the pion production region, in particular at higher energy, is the most important one.

A lower estimate is obtained by using the following assumptions (all assuming a carbon target): (a) In the giant-resonance region we use the experimental (γ,n) cross section; (b) in the quasideuteron region up to the pion threshold we take the branching ratio to be unity, since mostly both a neutron and a proton are emitted simultaneously; (c) in the region of pion production we assume that by quasifree processes there is always a primary branching ratio of 1/2 for neutron emission (equal number of neutrons and protons), while secondary absorption of negative pions give an additional branching ratio of $1.8n_{\pi^-}$, since stopping π^- gives a neutron pair in 80% and a neutron-proton pair in 20% of the cases. That is almost certainly an underestimate, particularly for large energy transfers ν for which a large number of hadrons is emitted in the reaction.

Our corresponding results for the neutron production underground are summarized in Table V, again divided into energy transfer bins of obvious physical significance. Even at very shallow depths the giant-resonance and quasideuteron regions contribute relatively little. As was the case of pion production, the asymptotic region, with its large uncertainty, appears not to be crucial for shallow depths ($d \leq 100$ m), but it gives a very significant fraction at deeper sites.

As far as comparison with the experiment is concerned two comments can be made. At $d = 20$ m in Ref. [5] two values are quoted. The total neutron yield is $(4\pm0.8)\times10^{-5}n$ per muon and per (g cm^{-2}). However, when the shower component (possibly originating from outside the detector) is eliminated, the neutron yield associated with muons alone is about 2 in the same units (and presumably with a similar error bar ±0.8 as above). Thus, our calculated number of 0.87 underestimates the neutron production by a factor of 2–4, indicating that secondary neutron production other than by pion capture is non-negligible even at such a shallow depth.

The depth dependence, as quoted in Ref. [17], suggests a fivefold increase at $d = 500$ m with a yield of about $2\times10^{-4}n$ per muon and per (g cm^{-2}). Our calculation therefore seriously underestimates the neutron yield at that depth, suggesting that secondary neutron production becomes crucial.

TABLE V. Summary of the primary neutron production yields in carbon [in units of $10^{-6}n$ per muon and per (g cm^{-2})].

Depth	Giant 0–30 MeV	Quasideuteron 30–150 MeV	Δ resonance 0.15–0.5 GeV	High energy 0.5–10 GeV	Asymptotic 10–100 GeV	Total
20 m	1.0	1.0	2.3	4.0	0.4	8.7
100 m	1.2	1.2	2.8	5.6	1.3	12.1
500 m	1.6	1.6	3.8	9.2	4.6	20.8

It is beyond the scope of this work to describe the secondary neutron production, and therefore the total neutron yields, quantitatively. We can, however, present some qualitative arguments. For bulk targets of heavy elements, the neutron multiplicities for hadron-induced processes at high energies increase linearly with the incident energy [18]. It is plausible that this linearity holds also for light elements. Since photons of energy larger than a few GeV have characteristic features of hadronic interactions (vector meson dominance), we may suppose that this linearity applies also in this case and is applicable even to the rather light elements of the detector of Ref. [17]. To determine empirically the unknown proportionality constant between the neutron multiplicity and the photon energy, we assume that below certain selected photon energy (i.e., muon energy loss) ν_0 our previous approach can be used, and above ν_0 the proportionality between the muon energy loss and the neutron yield holds. In order to fit the data [17] we need a multiplicity of four neutrons per GeV of photon energy for $\nu_0 = 2$ GeV or five neutrons per GeV for $\nu_0 = 10$ GeV. Our considerations, besides giving a lower limit for the neutron yield, offer a hint of the scenario which might emerge from such a description.

IV. CONCLUSIONS

In summary we have investigated the production of positive pions and neutrons by cosmic muons at underground sites of various depths. We have used the equivalent photon method, the validity of which we have tested in the case of a Δ isobaric model. We have made an exact evaluation of both the muon and photon cross sections in the framework of a specific model for Δ excitation. We have found that the equivalent photon method with a Dalitz-Yennie formula for the photon number reproduces remarkably well the theoretical cross section for the Δ excitation by muons, when the momentum dependence of the transverse response is neglected as well as the longitudinal response. This agreement is somewhat unexpected because of the momentum dependence of a response of magnetic type. Our investigation shows that the agreement is to a large part due to the effect of the form factors which cut off the large momenta. This success has led us to apply the Dalitz-Yennie formula (10) also in the region of the response where it has not been tested.

We then used the method to evaluate the production of positive pions in liquid scintillator from known photoabsorption cross sections. This estimate requires the knowledge of the branching ratio of the pion channel including the multiplicity. We find that at a depth of 20 m our estimate reproduces the measurement of Ref. [5].

As for the neutron production, we have shown that the low-energy mechanisms (giant-dipole excitation, quasideuteron production) are unimportant. Neutrons associated with pions appear to be the dominant source. However, using the information from the neutron production in direct processes together with neutrons produced from the absorption of stopped negative pions, our conservative estimates underpredict the experimentally observed neutron yield. This indicates that there is considerable secondary neutron production in the target environment. The quantitative description of such nuclear cascades is a formidable problem. Therefore, direct pion production is a much better test of our understanding of cosmic muon interactions, while the total neutron yield has a direct practical interest as a source of background at underground sites.

ACKNOWLEDGMENTS

We are grateful to Prof. J. Ahrens for data on photoproduction cross sections at high energy, and to Ralph Hertenberger and Mark Chen for numerous discussions regarding their experiment. Part of this work was done while two of us, M.E. and T.E., were visiting Caltech. We would like to thank Prof. Felix Boehm and Caltech for their hospitality. This work was supported in part by the U.S. Department of Energy under Grant No. DE-FG03-88ER40397.

[1] C. F. Weizsäcker, Z. Phys. **88**, 612 (1934).
[2] E. J. Williams, Kgl. Dan. Vidensk. Selsk. Mat. Fys. Medd. **XIII**, 4 (1935).
[3] R. H. Dalitz and D. R. Yennie, Phys. Rev. **105**, 1598 (1957).
[4] J. S. O'Connel and F. J. Schima, Phys. Rev. D **38**, 2277 (1988).
[5] R. Hertenberger, M. Chen, and B. L. Dougherty, Phys. Rev. C (submitted).
[6] F. E. Close, *An Introduction to Quarks and Partons* (Academic Press, London, 1979).
[7] J. J. Sakurai, Phys. Rev. Lett. **22**, 981 (1969).
[8] J. D. Jackson, *Classical Electrodynamics* (John Wiley, New York, 1963); see Eq. (15.56).
[9] G. Chanfray, J. Delorme, M. Ericson, and A. Molinari, Nucl. Phys. **A556**, 439 (1993).
[10] T. K. Gaisser, *Cosmic Rays and Particle Physics* (Cambridge Univ. Press, Cambridge, England, 1990).
[11] R. K. Adair and H. Kasha, in *Muon Physics I*, edited by V. W. Hughes and C. S. Wu (Academic Press, New York, 1977).
[12] J. M. Wyckoff, B. Ziegler, H. W. Koch, and R. Uhlig, Phys. Rev. **137**, B576 (1965).
[13] J. Ahrens, Nucl. Phys. **A446**, 229c (1985).
[14] *Data on* (γ,n) (γ,p) *and* (γ,d) *cross sections*, edited by H. Schopper, Landolt-Börstein, New Series, Group I, Vol. 12b (Springer, Berlin, 1988).
[15] L. W. Jones and K. M. Terwilliger, Phys. Rev. **91**, 699 (1953).
[16] R. I. Enikeev *et al.*, Sov. J. Nucl. Phys. **46**, 883 (1988).
[17] M. Aglietta *et al.*, Nuovo Cimento **12C**, 467 (1989).
[18] R. G. Vasilkov, V. I. Goldanski'i, and V. V. Orlov, Sov. J. Usp. **26**, 228 (1983).